Supplementary Information: Accurate machine learning force fields with experimental and simulation data fusion

Sebastien Röcken[1] and Julija Zavadlav [1,2]

[1] *Multiscale Modeling of Fluid Materials, Department of Engineering Physics and Computation, TUM School of Engineering and Design, Technical University of Munich, Germany*
[2] *Munich Data Science Institute, Technical University of Munich, Germany*

DFT database

We reuse the DFT database for titanium [1, 2]. Surface structures and γ-line defects are omitted from the database as they are not directly relevant to our target properties. We ensure that the box length is greater than twice the cutoff of the GNN. Samples with 16 atoms are periodically enlarged, once in the x and z-dimension and twice in the y-dimension. Samples with 32 atoms are enlarged once in every dimension. The new samples all contain 256 atoms. We then remove all samples with a box length smaller than twice the cutoff. Additionally, a few samples in this dataset were identified as outliers and removed. The remaining dataset consists of 5704 samples, which we split into 70% training, 10% validation, and 20% testing.

EXP database

We compute the experimental lattice constants by taking the experimental value at 298 K [3] and use the thermal expansion to compute the remaining ones. For the thermal expansion, we use values presented in Souvatzis et al. [4], taking the experimental thermal expansion by Nizankovski et al. [5] and fitting it to give the volume expansion by Mal'ko et al. [6].

DimeNet++ architecture hyperparameters

Hyperparameter	Value
Standard embedding size	32
Output embedding size	64
Triplet and atom-type embedding size	16
Bessel basis embedding	8
Cutoff length	0.5 nm
Interaction layers	4
Fully connected output layers	3
Residual blocks before skipping connection	1
Residual blocks after skipping connection	2
Radial Bessel embedding functions with a 6th order continuously differentiable envelop function	6
Angular Bessel embedding functions with a 6th order continuously differentiable envelop function	7
Activation function	Swish [7]
Weight Initialization	Orthogonal Gloro [8]

Table S1: Employed hyperparameters for DimeNet++.

Numerical optimization hyperparameters

We use the Adam optimizer with exponential learning rate decay (Table S2). For the DFT pre-trained model, we pick the model that performs best on the validation dataset. For the DFT, EXP sequential, DFT & EXP fused,

and DFT & EXP (323 K) fused model, we employ early stopping, i.e., we save the parameters every 10th epoch and pick the model with the lowest EXP training loss, only considering the elastic constant contribution, i.e., $\omega_P = 0$.

Hyperparameters	DFT pre-trained DFT trainer	DFT, EXP sequential EXP trainer	DFT & EXP fused DFT trainer	DFT & EXP fused EXP trainer
Initial learning rate	1e-3	2e-4	5e-7	2e-4
Learning rate decay	1e-2	1e-1	1e-2	1e-1
Number of epochs	400	200	200	200
Batch size	30	4	30	4

Hyperparameters	DFT & EXP (323 K) fused DFT trainer	DFT & EXP (323 K) fused EXP trainer
Initial learning rate	5e-7	2e-4
Learning rate decay	1e-2	1e-1
Number of epochs	200	200
Batch size	30	1

Table S2: Hyperparameters of the Adam optimizer.

Additional results

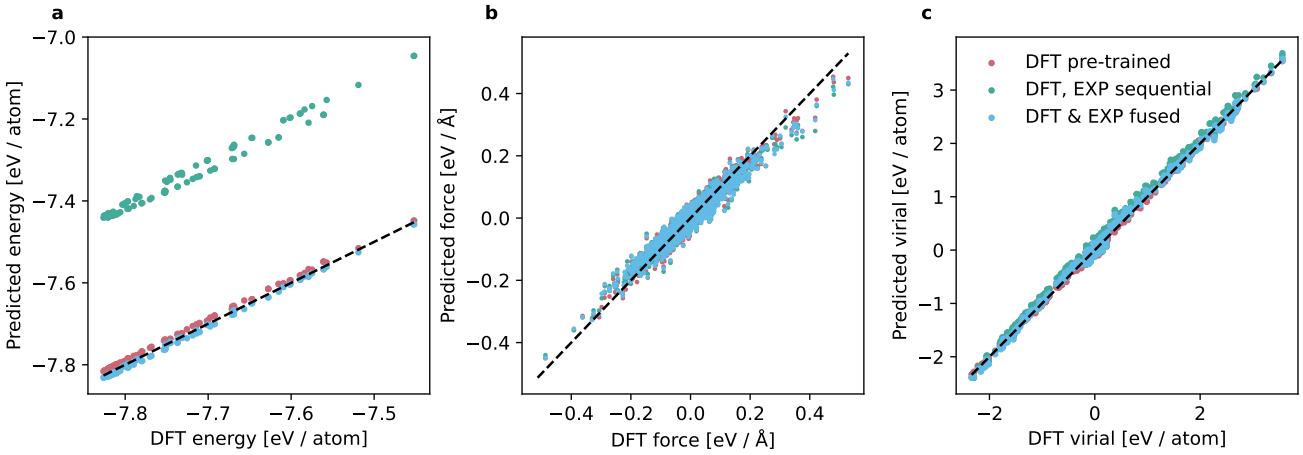

Figure S1: Predicted vs. DFT energy (**a**), force (**b**), and virial (**c**) for hcp titanium test samples, containing only strained and perturbed super cells. The predictions of the DFT pre-trained, DFT, EXP sequential, and DFT & EXP fused models are denoted with red, green, and blue points, respectively. All force/virial components are merged on the same plot. For forces, we show for clarity only every 50th sample.

	RMSE/MAE					
	hcp			bcc		
Model	Energy [meV/atom]	Force [meV/Å]	Virial [meV/atom]	Energy [meV/atom]	Force [meV/Å]	Virial [meV/atom]
DFT pre-trained	10.6/10.4	19.9/14.9	40.3/29.3	5.1/1.6	12.1/8.1	19.1/14.4
DFT, EXP sequential	386.4/386.2	22.4/16.9	81.4/55.0	363.7/363.5	13.5/9.6	81.7/44.9
DFT & EXP fused	6.6/5.6	23.1/17.7	49.0/35.2	10.2/9.4	13.3/9.2	22.3/16.3
Wen et al.*	1.4/-	29.2/-	-/-	0.5/-	15.3/-	-/-

Table S3: Root Mean Square Error (RMSE) and Mean Absolute Error (MSE) of energy, force, and virial computed only for hcp and bcc test dataset samples, containing only strained and perturbed super cells. *Results are taken from Ref. [1]. A comparison should be taken with care since the used DFT datasets are not exactly the same, i.e., we omitted some structures as written above.

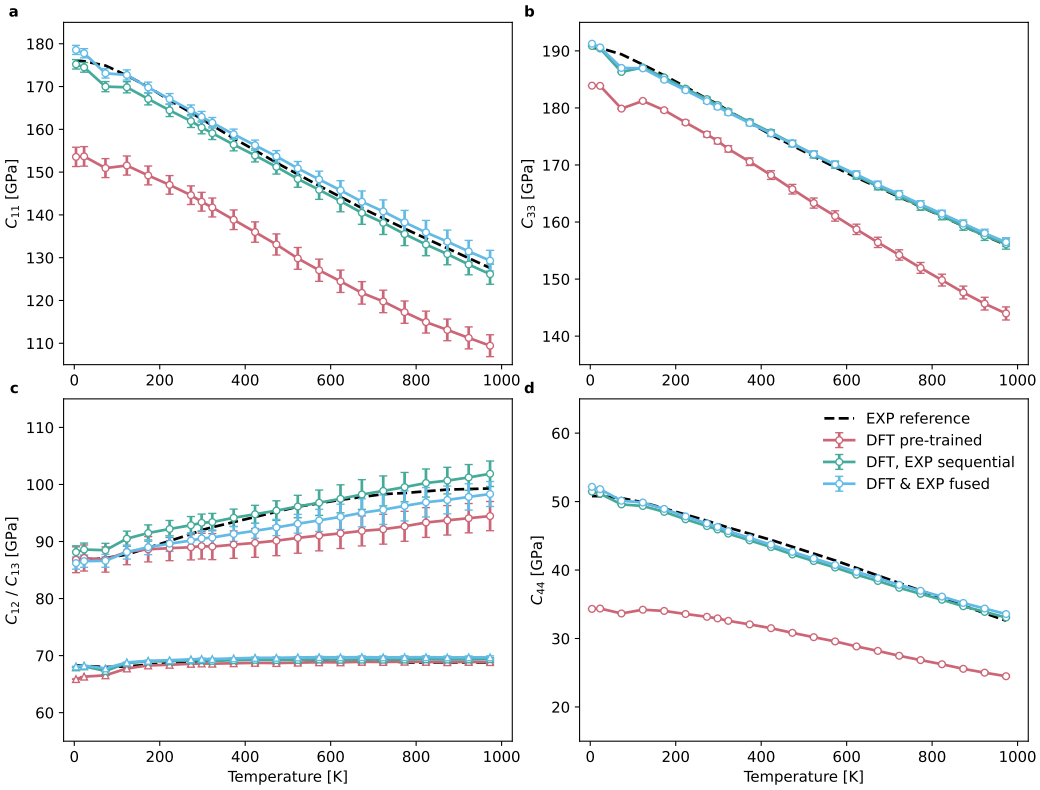

Figure S2: Elastic constants C_{11} (**a**), C_{33} (**b**), C_{12} (**c**, circle), C_{13} (**c**, triangle), and C_{44} (**d**) of hcp titanium in Voigt notation as a function of temperature. The DFT pre-trained, DFT, EXP sequential, and DFT & EXP fused models are denoted with red, green, and blue line points, respectively. The experimental results are denoted with a black dashed line. Error bars denote the standard deviation computed via block-averaging with 10 blocks.

Model	C_{11}	C_{12}	C_{13}	C_{33}	C_{44}	K	G	ν
DFT pre-trained	13.1	3.8	0.8	4.9	29.1	6.1	24.4	8.9
DFT, EXP sequential	1.1	**1.3**	**0.5**	**0.2**	1.6	**0.2**	2.1	0.9
DFT & EXP fused	**0.8**	1.7	0.7	0.3	**1.2**	0.2	**1.4**	**0.5**

Table S4: Relative deviation in percentage of the predicted hcp elastic constants C_{**} in Voigt notation, bulk modulus (K), shear modulus (G), and Poisson's ratio (ν) from the experimental reference.

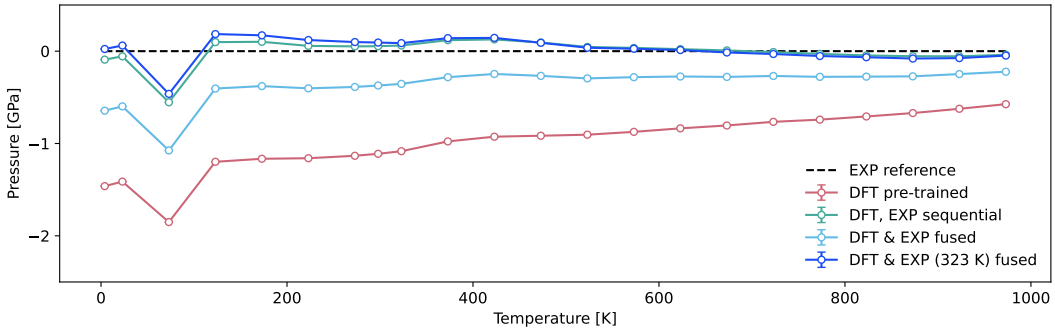

Figure S3: Predicted pressure as a function of temperature. The DFT pre-trained, DFT, EXP sequential, DFT & EXP fused, and DFT & EXP (323 K) fused models are denoted with red, green, blue, and dark blue line points, respectively. The black dashed line marks the zero pressure target.

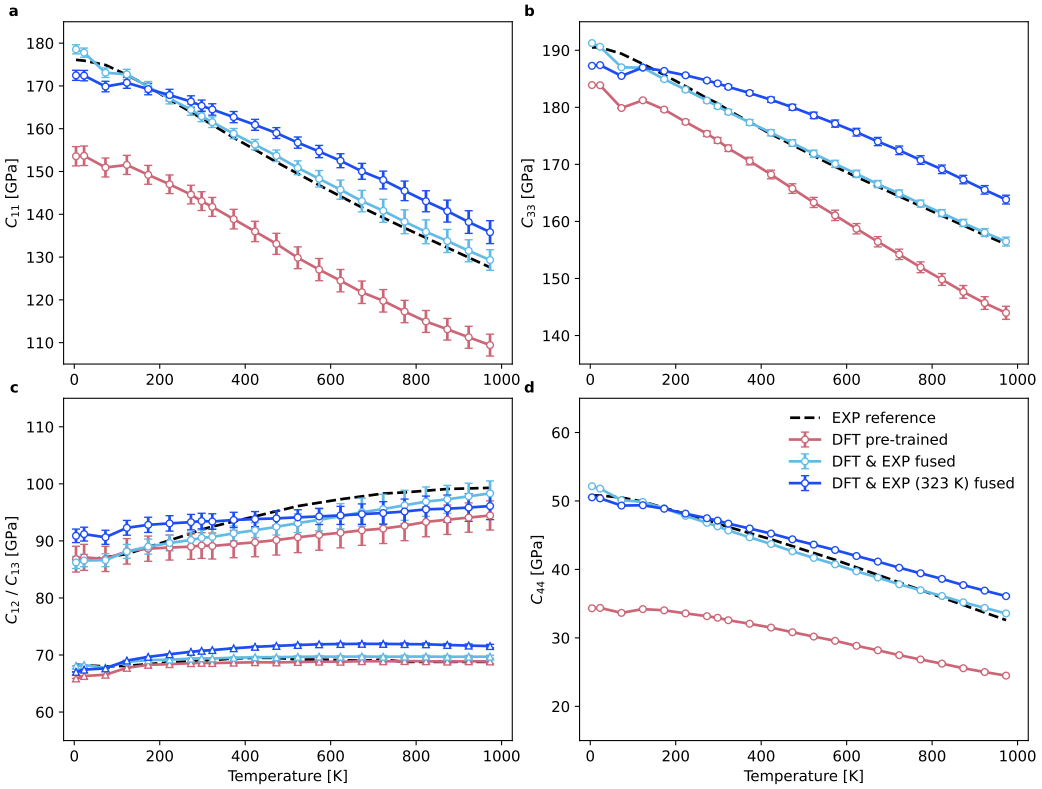

Figure S4: Elastic constants C_{11} (**a**), C_{33} (**b**), C_{12} (**c**, circle), C_{13} (**c**, triangle), and C_{44} (**d**) of hcp titanium in Voigt notation as a function of temperature. The DFT pre-trained, DFT & EXP fused, and DFT & EXP (323 K) fused models are denoted with red, blue, and dark blue line points, respectively. The experimental results are denoted with a black dashed line. Error bars denote the standard deviation computed via block-averaging with 10 blocks.

References

[1] Wen, T. *et al.* Specialising neural network potentials for accurate properties and application to the mechanical response of titanium. *npj Computational Materials* **7**, 206 (2021).

[2] `https://www.aissquare.com/datasets/detail?pageType=datasets&name=Ti`. Accessed: 2023-07-21.

[3] Barrett, C. S. & TB, M. Structure of metals. crystallographic methods, principles and data (1980).

[4] Souvatzis, P., Eriksson, O. & Katsnelson, M. Anomalous thermal expansion in α-titanium. *Physical review letters* **99**, 015901 (2007).

[5] Trefilov, A. Anisotropy of the thermal expansion of titanium due to proximity to an electronic topological transition. *JETP lett* **59** (1994).

[6] Mal'ko, P., Arensburger, D., Pugin, V., Nemchenko, V. & L'vov, S. Thermal and electrical properties of porous titanium. *Soviet Powder Metallurgy and Metal Ceramics* **9**, 642–644 (1970).

[7] Ramachandran, P., Zoph, B. & Le, Q. V. Searching for activation functions. *arXiv preprint arXiv:1710.05941* (2017).

[8] Glorot, X. & Bengio, Y. *Understanding the difficulty of training deep feedforward neural networks*, 249–256 (JMLR Workshop and Conference Proceedings, 2010).